

Robust 6G OFDM High-Mobility Communications Using Delay-Doppler Superimposed Pilots

Mauro Marchese[✉], *Graduate Student Member, IEEE*, Pietro Savazzi[✉], *Senior Member, IEEE*

Abstract—In this work, a novel receiver architecture for orthogonal frequency division multiplexing (OFDM) communications in 6G high-mobility scenarios is developed. In particular, a delay-Doppler superimposed pilot (SP) scheme is used for channel estimation (CE) by adding a single pilot in the delay-Doppler domain. Unlike previous research on delay-Doppler superimposed pilots in OFDM systems, intercarrier interference (ICI) effects, fractional delays, and Doppler shifts are considered. Consequently, a disjoint fractional delay-Doppler estimation algorithm is derived, and a reduced-complexity equalization method based on the Landweber iteration, which exploits intrinsic channel structure, is proposed. Simulation results reveal that the proposed receiver architecture achieves robust communication performance across various mobility conditions, with speeds of up to 1000 km/h, and increases the effective throughput compared to existing methods.

Index Terms—OFDM, superimposed pilots, channel estimation, equalization.

I. INTRODUCTION

TODAY, wireless communication systems widely adopt the orthogonal frequency division multiplexing (OFDM) waveform to achieve high spectral efficiency and robust performance. The attractiveness of OFDM stems from its resilience to intersymbol interference (ISI) in multipath environments [1], [2]. In particular, the use of the cyclic prefix (CP) guarantees ISI-free operation, provided that the CP length is designed to be greater than the channel delay spread. As a consequence, subcarrier orthogonality remains intact, and the per-subcarrier channels can be modeled as additive white gaussian noise (AWGN) channels. However, this optimal performance is experienced only in static multipath channels. When mobility occurs, the channel becomes time-varying [2]. Under low-mobility conditions, the channel frequency response (CFR) changes slowly over time and can be considered constant within one OFDM symbol. In such cases, OFDM can achieve near-optimal performance, as the time-frequency resource elements (REs) remain almost orthogonal at the receiver. Therefore, the simple and well-known single-tap equalizer can be adopted at the receiver [2], [3].

In recent years, high-mobility communications have become increasingly important for the development of next-generation wireless systems, such as 6G vehicle-to-everything (V2X), high-speed railways (HSR), and unmanned aerial vehicles

M. Marchese is with the Department of Electrical, Computer and Biomedical Engineering, University of Pavia, Pavia, 27100 Italy (e-mail: mauro.marchese01@universitadipavia.it).

Pietro Savazzi is with the Department of Electrical, Computer and Biomedical Engineering, University of Pavia, Pavia, 27100 Italy (e-mail: pietro.savazzi@unipv.it), and with the Consorzio Nazionale Interuniversitario per le Telecomunicazioni - CNIT.

(UAVs). In these scenarios, speeds of up to 1000 km/h [4], [5] can be experienced, and Doppler effects become prominent. Under such conditions, orthogonality is destroyed by intercarrier interference (ICI) [6]–[9], and the performance of OFDM degrades. Moreover, the advantage of low-complexity symbol detection via single-tap equalization vanishes, as more complex equalization methods, such as minimum mean squared error (MMSE) [10], [11], must be adopted. As a consequence, novel waveforms have been introduced to overcome the limitations of OFDM [12]. In particular, a waveform known as orthogonal time frequency space (OTFS) was proposed in [13] and has garnered significant attention due to its performance gains over OFDM. OTFS operates in the delay-Doppler domain [2], [13], [14], where the channel can be considered sparse and nearly time-invariant [2], [13].

Accordingly, several works have addressed OTFS channel estimation (CE) in the delay-Doppler domain by using either dedicated pilots [15]–[19] or superimposed pilots (SPs) [20], [21]. In OTFS, the CE problem is formulated as a parameter estimation problem, where the objective is to estimate the channel parameters, namely the channel gains, delays, and Doppler shifts.

On the other hand, conventional CE schemes in OFDM systems rely on embedded-pilots (EPs) in the time-frequency domain and directly estimate the channel response at pilot positions, followed by interpolation to recover the full channel response [22], [23]. SP-based schemes for OFDM systems have also been investigated in [24]–[30]. In these works, frequency-domain pilots are linearly superimposed onto data symbols across subcarriers.

More recently, the idea of incorporating OTFS-like delay-Doppler processing into OFDM systems has attracted increasing attention, as it allows one to exploit the channel properties in the delay-Doppler domain, namely sparsity and the large geometric coherence time of the channel parameters (channel gains, propagation delays, and Doppler shifts) [2]. In [31], [32], parameter-based channel estimation is performed by transmitting dedicated pilots in the time-frequency domain, achieving more robust communication performance. Similarly, in [11], a delay-Doppler aided OFDM (DD-a-OFDM) scheme is proposed for high-mobility scenarios by exploiting CE in the delay-Doppler domain together with conventional MMSE equalization in the time-frequency domain.

In [3], a novel pilot scheme for OFDM that exploits the superposition of pilots in the delay-Doppler domain is proposed. Specifically, a single delay-Doppler pilot is superimposed onto the time-frequency OFDM symbol matrix, and channel estimation is performed by searching for peaks in the delay-Doppler domain, in a manner similar to OTFS-

based SP channel estimation [20], [21]. This approach is sometimes referred to as threshold method (TM) in the OTFS literature [2], [18], [19]. However, the work in [3] relies on two simplifying assumptions: (i) ICI-free operation, such that the channel is constant within an OFDM symbol and single-tap equalization can be employed at the receiver; and (ii) integer delays and Doppler shifts, implying that the channel parameters are multiples of the delay and Doppler resolutions. In practical 6G high-mobility scenarios, these assumptions do not generally hold. Therefore, the following question arises: *is it possible to achieve robust communication performance in 6G OFDM high-mobility scenarios in the presence of ICI and fractional channel parameters by leveraging delay-Doppler SP schemes?* This work aims to address this question by: (i) relaxing the integer delay-Doppler assumption in [3] and developing a novel delay-Doppler SP-based CE algorithm for OFDM; and (ii) introducing an ICI-aware equalization scheme for OFDM with lower computational complexity than the conventional full-MMSE detector [10], [11].

A. Contributions

Given the above discussion, the contributions of this work are summarized as follows:

- **Novel fractional delay-Doppler estimation based on a SP scheme:** By relaxing the oversimplifying assumptions made in [3], a novel algorithm for disjoint estimation of fractional delays and Doppler shifts is developed. In particular, under the proposed delay-Doppler superimposed pilot scheme, the integer components are obtained by searching for the maximum pilot energy in the delay-Doppler domain. Subsequently, fractional delays and Doppler shifts are estimated by correlating the received profiles with the corresponding delay and Doppler terms. This approach enhances CE performance in realistic scenarios with fractional channel parameters, while maintaining the low computational complexity inherited from the disjoint estimation process.

- **Low-complexity equalization based on the Landweber method:** A path-wise low-complexity equalizer, termed iterative matched filtering and combining (IMFC), based on the Landweber algorithm [33], [34], is developed for symbol detection. Specifically, the intrinsic structure of the channel is exploited to decompose the iterative algorithm into multiple low-complexity operations. The computational complexity of this approach scales linearly with the number of time-frequency REs, in contrast to the conventional MMSE equalizer, whose complexity scales cubically with the number of subcarriers [10], [11].

- **Mobility-resilient numerical analysis under ICI and fractional delays and Doppler shifts:** Extensive simulations are conducted to evaluate the robustness of the proposed delay-Doppler SP-based OFDM receiver against mobility in practical scenarios characterized by ICI and fractional channel parameters. Different modulation formats, signal-to-noise ratios (SNRs), and user speeds are considered. The numerical results demonstrate the robustness of the proposed OFDM receiver against

mobility. In particular, the proposed scheme achieves an approximately constant effective throughput over a wide range of maximum speeds, up to 1000 km/h, which corresponds to the maximum velocity targeted by 6G networks [4], [5].

Notation: x is a scalar, \mathbf{x} is a vector, and \mathbf{X} is a matrix. The (m, n) -th element of matrix \mathbf{X} is denoted as $[\mathbf{X}]_{m,n}$. For a matrix \mathbf{X} , $[\mathbf{X}]_{:,n}$ and $[\mathbf{X}]_{m,:}$ denote the n -th column and the m -th row of \mathbf{X} , respectively. \mathbf{X}^* , \mathbf{X}^\top , \mathbf{X}^H and \mathbf{X}^{-1} represent the complex conjugate, transpose, Hermitian (conjugate transpose) and inverse of \mathbf{X} . Moreover, $\|\mathbf{X}\|_F$ and $\text{Tr}(\mathbf{X})$ represent the Frobenius norm and the trace of \mathbf{X} , respectively. The operator $\text{diag}(\mathbf{x})$ denotes the diagonal matrix whose main diagonal is given by the elements of vector \mathbf{x} . \mathbf{I}_N denotes the identity matrix of order N . The notation $[\cdot]_N$ indicates the modulo- N operation. \odot and \circledast represent Hadamard (element-wise) and 2D circular convolution, respectively. The expectation operator is denoted as $\mathbb{E}[\cdot]$. The distribution $\mathcal{CN}(\mu, \Sigma)$ denotes a circularly symmetric complex Gaussian random vector with mean μ and covariance matrix Σ . Finally, δ_{ij} is the Kronecker delta that takes the value 1 when $i = j$ and zero otherwise.

II. SYSTEM MODEL

In this section, the single-input single-output (SISO) OFDM system model is presented, and both ICI-aware and ICI-free models are discussed.

A. Continuous-Time Model

1) *OFDM Transmit Signal Model:* The transmitter (TX) arranges $M \times N$ symbols in the time-frequency plane across M subcarriers with spacing Δf and N time slots. Accordingly, the transmit symbol matrix $\mathbf{X} \in \mathbb{C}^{M \times N}$ is obtained. Denoting $[\mathbf{X}]_{m,n} = x_{m,n}$ as the (m, n) -th RE, the transmit signal during the n -th symbol duration is given by [35]

$$s_n(t) = \frac{1}{\sqrt{M}} \sum_{m=0}^{M-1} x_{m,n} e^{j2\pi m \Delta f t} \Pi\left(\frac{t - nT'}{T'}\right), \quad (1)$$

where $\Pi(t)$ is a rectangular pulse that takes the value 1 for $t \in [0, 1]$ and 0 otherwise, and T' denotes the overall OFDM symbol duration. Specifically, $T' = T + T_{\text{CP}}$, where $T = 1/\Delta f$ and $T_{\text{CP}} > \sigma_\tau$ denotes the duration of the CP, with σ_τ being the channel delay spread. Therefore, as in standard OFDM transmission, ISI is avoided. In the following, the overall signal including the CP is denoted by $s_n^{\text{CP}}(t)$.

2) *Channel Model:* The high-mobility wireless channel consists of P propagation paths, each characterized by a delay τ_p , a Doppler shift ν_p , and a complex channel gain α_p . The time-varying impulse response of the SISO channel is given by

$$h(t, \tau) = \sum_{p=1}^P \alpha_p e^{j2\pi \nu_p t} \delta(\tau - \tau_p). \quad (2)$$

3) *Received Signal Model*: During the n -th symbol interval, the received signal is expressed as

$$\begin{aligned} r_n^{\text{CP}}(t) &= \int h(t, \tau) s_n^{\text{CP}}(t - \tau) d\tau + n(t) \\ &= \sum_{p=1}^P \alpha_p s_n^{\text{CP}}(t - \tau_p) e^{j2\pi\nu_p t} + n(t), \end{aligned} \quad (3)$$

where $n(t)$ denotes AWGN with one-sided power spectral density (PSD) N_0 .

B. ICI-Aware Model in Matrix Form

By sampling (1) at the symbol rate T/M , the transmit signal vector is given by

$$\mathbf{s}_n = \mathbf{F}_M^H \mathbf{x}_n \in \mathbb{C}^{M \times 1}, \quad (4)$$

where $[\mathbf{F}_M]_{m,q} = \frac{1}{\sqrt{M}} e^{-j2\pi \frac{mq}{M}}$ denotes the M -point discrete Fourier transform (DFT) matrix. Moreover, the average transmit power is defined as $P_T = \mathbb{E}[\|\mathbf{S}\|_F^2]/(MN)$, where $\mathbf{S} = [\mathbf{s}_0 \mathbf{s}_1 \dots \mathbf{s}_{N-1}] \in \mathbb{C}^{M \times N}$ denotes the transmit signal matrix.

Similarly, by sampling (3) at the same rate and removing the CP, the received observation vectors $\mathbf{r}_n \in \mathbb{C}^{M \times 1}$ are obtained as [35], [36]

$$\mathbf{r}_n = \mathbf{H}_n \mathbf{s}_n + \mathbf{n}_n, \quad (5)$$

where $\mathbf{n}_n \sim \mathcal{CN}(\mathbf{0}, \sigma^2 \mathbf{I}_M)$ denotes the AWGN vector, and $\mathbf{H}_n \in \mathbb{C}^{M \times M}$ is the channel matrix given by

$$\mathbf{H}_n = \sum_{p=1}^P \tilde{\alpha}_{p,n} \tilde{\mathbf{C}}(\nu_p) \mathbf{F}_M^H \mathbf{B}(\tau_p) \mathbf{F}_M. \quad (6)$$

Here, $\mathbf{B}(\tau) = \text{diag}(\mathbf{b}(\tau))$, with $\mathbf{b}(\tau) = [e^{-j2\pi q\tau \Delta f}]_{q=0}^{M-1}$, and $\tilde{\mathbf{C}}(\nu) = \text{diag}(\tilde{\mathbf{c}}(\nu))$, where $\tilde{\mathbf{c}}(\nu) = [e^{j2\pi q\nu \frac{T}{M}}]_{q=0}^{M-1}$ captures fast-time variations due to Doppler, i.e., ICI. Furthermore, $\tilde{\alpha}_{p,n} = \alpha_p e^{j2\pi\nu_p t_n}$ denotes the Doppler-induced time-varying channel gain, where $t_n = T_{\text{CP}} + nT'$ is the time instant at which the transmission of the n -th OFDM symbol starts. This term captures the slow-time variations induced by Doppler.

By concatenating the received observation vectors as $\mathbf{R} = [\mathbf{r}_0 \mathbf{r}_1 \dots \mathbf{r}_{N-1}]$, the received OFDM frame can be expressed as [35]

$$\mathbf{R} = \sum_{p=1}^P \alpha_p \tilde{\mathbf{C}}(\nu_p) \mathbf{F}_M^H \left(\mathbf{X} \odot \mathbf{b}(\tau_p) \mathbf{c}^\top(\nu_p) \right) + \mathbf{N} \in \mathbb{C}^{M \times N}, \quad (7)$$

where $\mathbf{c}(\nu) \in \mathbb{C}^{N \times 1}$ is the slow-time Doppler steering vector defined as $\mathbf{c}(\nu) = [e^{j2\pi\nu t_n}]_{n=0}^{N-1}$, and $\mathbf{N} = [\mathbf{n}_0 \mathbf{n}_1 \dots \mathbf{n}_{N-1}]$ denotes the noise matrix.

The input-output relation in (7) can be compactly rewritten as

$$\mathbf{R} = \mathcal{H}(\mathbf{X}) + \mathbf{N}, \quad (8)$$

where $\mathcal{H}(\cdot) = \sum_{p=1}^P \alpha_p \left[\mathbf{F}_M^H ((\cdot) \odot \mathbf{H}_{\text{tf}}^{(p)}) \odot \mathbf{H}_{\text{ICI}}^{(p)} \right]$ denotes the channel operator. Moreover, $\mathbf{H}_{\text{tf}}^{(p)}$ is the frequency-time

channel matrix associated with the p -th propagation path, given by

$$\mathbf{H}_{\text{tf}}^{(p)} = \mathbf{b}(\tau_p) \mathbf{c}^\top(\nu_p), \quad (9)$$

and $\mathbf{H}_{\text{ICI}}^{(p)}$ is the delay-time ICI matrix accounting for the ICI generated by the p -th path, defined as

$$\mathbf{H}_{\text{ICI}}^{(p)} = \tilde{\mathbf{c}}(\nu_p) \mathbf{1}_N^\top. \quad (10)$$

C. ICI-Free Model in Matrix Form

The model in (7) simplifies when the subcarrier spacing satisfies $\Delta f \gg \nu_{\text{max}}$, where $\nu_{\text{max}} = \frac{v_{\text{max}}}{c}$, and v_{max} and f_c denote the maximum speed and the carrier frequency, respectively. Under this condition, ICI becomes negligible, such that $\tilde{\mathbf{C}}(\nu) \approx \mathbf{I}_M$, and the well-known ICI-free model is obtained [3]

$$\mathbf{R} = \mathbf{F}_M^H \sum_{p=1}^P \alpha_p \left(\mathbf{X} \odot \mathbf{b}(\tau_p) \mathbf{c}^\top(\nu_p) \right) + \mathbf{N}. \quad (11)$$

Moreover, by transforming the delay-time observations in (11) to the frequency-time domain, one obtains

$$\mathbf{Y} = \mathbf{F}_M \mathbf{R} = \mathbf{H}_{\text{tf}} \odot \mathbf{X} + \mathbf{N}, \quad (12)$$

where the frequency-time channel matrix is given by [3]

$$\mathbf{H}_{\text{tf}} = \sum_{p=1}^P \alpha_p \mathbf{b}(\tau_p) \mathbf{c}^\top(\nu_p). \quad (13)$$

In this case, the receiver can employ a single-tap equalizer to compensate for the channel effects.

III. CHANNEL ESTIMATION WITH DELAY-DOPPLER SUPERIMPOSED PILOTS

This section first presents the conventional EP method for channel estimation, followed by the delay-Doppler superimposed pilot model proposed in [3] for CE in OFDM systems. Subsequently, the threshold method used in [3] is reviewed, and its limitations are discussed. Finally, the proposed iterative CE algorithm accounting for fractional channel parameters is presented.

A. Conventional Channel Estimation in the Time-Frequency Domain using Embedded Pilots

The conventional channel estimation scheme in OFDM systems assumes negligible ICI and therefore relies on the ICI-free model in (12). Channel estimation is based on dedicated pilots in the time-frequency domain, commonly referred to as the EP scheme. In this method, pilot symbols are allocated to specific REs to maximize the SNR and minimize pilot-data interference. The channel is first estimated at pilot locations and then reconstructed over the entire time-frequency grid using interpolation techniques applied to (13).

Specifically, pilots are inserted into the time-frequency grid according to a defined periodicity along both frequency and time, resulting in a non-zero pilot density \mathcal{D}_p [3]. The pilot density is defined as

$$\mathcal{D}_p = \frac{1}{K_t K_f}, \quad (14)$$

where K_f and K_t denote the spacings between pilots along the frequency and time axes, respectively. The transmitted signal matrix \mathbf{X} contains pilot symbols in dedicated positions \mathcal{X}_p , which carry known information, and data symbols (e.g., quadrature amplitude modulation (QAM)) occupying the remaining REs \mathcal{X}_d . Accordingly, \mathbf{X} is constructed as

$$x_{m,n} = \begin{cases} \text{pilot,} & \forall (m,n) \in \mathcal{X}_p, \\ \text{data,} & \forall (m,n) \in \mathcal{X}_d. \end{cases} \quad (15)$$

Channel estimation in the dedicated pilot scheme is typically performed in two steps: first, estimation at pilot locations, and second, interpolation across the data REs.

1) *Channel Estimation at Pilot Locations*: The channel response is estimated only at the pilot locations $(m, n) \in \mathcal{X}_p$. Given the received time-frequency signal in (12), the least squares (LS) estimate of the channel at pilot locations is given by

$$[\hat{\mathbf{H}}_{\text{tf}}]_{m,n} = \frac{[\mathbf{Y}]_{m,n}}{x_{m,n}}, \quad \forall (m,n) \in \mathcal{X}_p. \quad (16)$$

2) *Channel Interpolation*: To obtain the complete channel state information (CSI) estimate $\hat{\mathbf{H}}_{\text{tf}}$ over the entire $M \times N$ grid, interpolation is required. Sequential linear interpolation is typically performed in two steps: first along one dimension (e.g., frequency) and then along the other dimension (time) using the results from the first step.

For a data RE (m', n) located between two adjacent pilots in the frequency domain at m_p and $m_p + K_f$, the interpolated estimate is

$$[\hat{\mathbf{H}}_{\text{tf}}]_{m',n} = [\hat{\mathbf{H}}_{\text{tf}}]_{m_p,n} + \frac{m' - m_p}{K_f} \left([\hat{\mathbf{H}}_{\text{tf}}]_{m_p+K_f,n} - [\hat{\mathbf{H}}_{\text{tf}}]_{m_p,n} \right). \quad (17)$$

After obtaining estimates across all subcarriers m' (from 0 to $M - 1$), the interpolation proceeds along the time dimension. For a data RE (m', n') located between two adjacent pilots in the time domain at n_p and $n_p + K_t$, the interpolation uses the estimates obtained from the previous step:

$$[\hat{\mathbf{H}}_{\text{tf}}]_{m',n'} = [\hat{\mathbf{H}}_{\text{tf}}]_{m',n_p} + \frac{n' - n_p}{K_t} \left([\hat{\mathbf{H}}_{\text{tf}}]_{m',n_p+K_t} - [\hat{\mathbf{H}}_{\text{tf}}]_{m',n_p} \right). \quad (18)$$

This procedure is applied sequentially along both dimensions to reconstruct the full $\hat{\mathbf{H}}_{\text{tf}}$ matrix.

The performance of the conventional EP scheme is limited by the Doppler-induced time-varying nature of the channel. In particular, in high-mobility scenarios, ICI destroys subcarrier orthogonality, causing the ICI-free EP scheme to fail.

B. Delay-Doppler Pilot Superimposition

In this section, the delay-Doppler SP scheme proposed in [3] is introduced. Figure 1 illustrates both the conventional EP approach and the delay-Doppler SP scheme considered in [3].

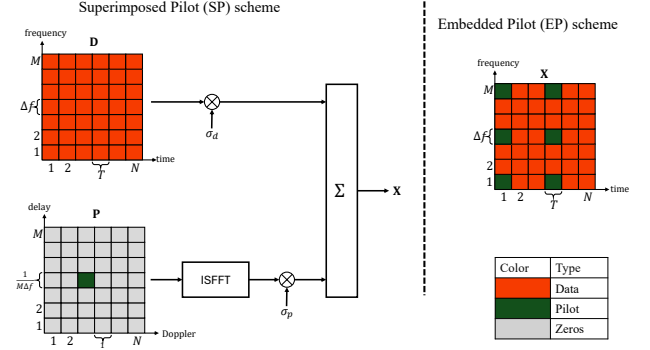


Fig. 1: The delay-Doppler superimposed pilot (SP) scheme and the conventional time-frequency embedded pilot (EP) scheme adopted in OFDM systems.

Let $\mathbf{P} \in \mathbb{C}^{M \times N}$ denote the delay-Doppler pilot matrix. A unit-amplitude pilot is placed for channel estimation as [3]

$$[\mathbf{P}]_{m,n} = \delta_{mm_p} \delta_{nn_p} = \begin{cases} 1, & m = m_p, n = n_p, \\ 0, & \text{otherwise,} \end{cases} \quad (19)$$

which can equivalently be expressed as

$$\mathbf{P} = \mathbf{e}_{m_p} \mathbf{e}_{n_p}^\top, \quad (20)$$

where $[\mathbf{e}_i]_j = \delta_{ij}$ denotes a one-hot vector with a single one at position i . It follows that $\|\mathbf{P}\|_F^2 = 1$.

This delay-Doppler pilot is superimposed onto OFDM frequency-time data via the inverse symplectic finite Fourier transform (ISFFT) as

$$\mathbf{X} = \sigma_d \mathbf{D} + \sigma_p \underbrace{\mathbf{F}_M \mathbf{P} \mathbf{F}_N^\text{H}}_{\text{ISFFT}} \in \mathbb{C}^{M \times N}, \quad (21)$$

where \mathbf{D} contains data symbols (e.g., QAM) with $\mathbb{E}[|d_{m,n}|^2] = 1$, where $d_{m,n} = [\mathbf{D}]_{m,n}$, so that $\mathbb{E}[\|\mathbf{D}\|_F^2] = MN$. Here, σ_d^2 and σ_p^2 denote the power allocated to data and pilot symbols, respectively.

Defining the channel gains vector as $\boldsymbol{\alpha} = [\alpha_1, \alpha_2, \dots, \alpha_P]^\top$ and assuming $\|\boldsymbol{\alpha}\|^2 = 1$, the SNR is given by

$$\begin{aligned} \text{SNR} &= \frac{P_T}{\sigma^2} = \frac{\mathbb{E}[\|\mathbf{X}\|_F^2]}{\mathbb{E}[\|\mathbf{N}\|_F^2]} \\ &= \frac{\sigma_d^2 \mathbb{E}[\|\mathbf{D}\|_F^2] + \sigma_p^2 \|\mathbf{P}\|_F^2}{\mathbb{E}[\|\mathbf{N}\|_F^2]} \\ &= \frac{MN\sigma_d^2 + \sigma_p^2}{MN\sigma^2} = \frac{\sigma_d^2 \left(1 + \frac{\beta}{MN}\right)}{\sigma^2}, \end{aligned} \quad (22)$$

where $\beta = \sigma_p^2/\sigma_d^2$ is the pilot-to-data ratio (PDR) and allows for boosting the pilot amplitude to facilitate channel estimation [3].

C. SP Channel Estimation Baseline: Threshold Method

As a baseline for channel estimation in OFDM systems using delay-Doppler superimposed pilots, the method proposed in [3] is considered. This method, referred to as the TM, relies on two simplifying assumptions: ICI-free operation and integer delays and Doppler shifts.

The received delay-Doppler samples \mathbf{Y}_{dd} are modeled as a circular convolution [2], [3]:

$$\mathbf{Y}_{dd} = \mathbf{F}_M^H \mathbf{Y} \mathbf{F}_N = \mathbf{H}_{dd} \circledast \mathbf{X}_{dd} + \mathbf{N}_{dd}, \quad (23)$$

where $\mathbf{H}_{dd} = \mathbf{F}_M^H \mathbf{H}_{tf} \mathbf{F}_N$ is the delay-Doppler channel matrix, and $\mathbf{X}_{dd} = \sigma_p \mathbf{P} + \sigma_d \mathbf{F}_M^H \mathbf{D} \mathbf{F}_N$ are the delay-Doppler samples.

Assuming integer delays and Doppler shifts [3], such that $\tau_p = l_p/(M\Delta f)$ and $\nu_p = k_p/(NT')$, where $l_p, k_p \in \mathbb{Z}$ denote the normalized delay and Doppler indices, the relation in (23) simplifies to

$$[\mathbf{Y}_{dd}]_{m,n} = \sum_{p=1}^P \alpha_p [\mathbf{X}_{dd}]_{[m-l_p]_M, [n-k_p]_N} + [\mathbf{N}_{dd}]_{m,n}. \quad (24)$$

Using the delay-Doppler superimposed pilot, channel parameters $\{\alpha_p, l_p, k_p\}_{p=1}^P$ are estimated by detecting peaks that exceed a predefined threshold \mathcal{T} [3], [21]. Specifically, a path with delay \hat{l}_p and Doppler \hat{k}_p is detected if

$$[\mathbf{Y}_{dd}]_{m_p+\hat{l}_p, n_p+\hat{k}_p} \geq \mathcal{T}, \quad (25)$$

and the channel gain is estimated from (24) as

$$\hat{\alpha}_p = \frac{[\mathbf{Y}_{dd}]_{m_p+\hat{l}_p, n_p+\hat{k}_p}}{\sigma_p}. \quad (26)$$

The time-frequency channel matrix is then reconstructed as

$$\hat{\mathbf{H}}_{tf} = \sum_{p=1}^{\hat{P}} \hat{\alpha}_p \mathbf{b}\left(\frac{\hat{l}_p}{M\Delta f}\right) \mathbf{c}^\top\left(\frac{\hat{k}_p}{NT'}\right), \quad (27)$$

where \hat{P} is the number of detected peaks exceeding the threshold \mathcal{T} . Following [21], the threshold is typically set as $\mathcal{T} = 3\sqrt{\sigma^2 + \sigma_d^2}$.

Remark 1. When channel parameters are not integers, the pilot signal spreads across adjacent delay-Doppler bins [2], [16]–[19]. This is the main limitation of the threshold method: a single multipath component with fractional parameters is approximated as multiple integer-valued components. Since only portions of the spread pilot exceeding the threshold are detected, some fractional multipath contributions may be missed. In contrast, channel estimation methods that explicitly account for fractional delays and Doppler shifts can accurately reconstruct the spreading effect, significantly improving estimation performance.

D. Proposed SP Channel Estimation Method Accounting for Fractional Channel Parameters

This section introduces the proposed CE scheme based on the ICI-aware model in (7).

1) *Single-path Scenario:* Considering a single-path channel and given the pilot model in (20), disjoint delay-Doppler estimation can be performed as follows. The received delay-Doppler matrix is given by

$$\mathbf{Y}_{dd} = \mathbf{R} \mathbf{F}_N = \alpha \tilde{\mathbf{C}}(\nu) \mathbf{F}_M^H \left(\mathbf{X} \odot \mathbf{b}(\tau) \mathbf{c}^\top(\nu) \right) \mathbf{F}_N + \mathbf{N}_{dd}. \quad (28)$$

The delay and Doppler of the path are first initialized by searching for the maximum pilot energy in the delay-Doppler matrix [16], [17], [19]:

$$\hat{l}, \hat{k} = \arg \max_{l,k} \left| [\mathbf{Y}_{dd}]_{m_p+l, n_p+k} \right|^2. \quad (29)$$

The delay and Doppler can then be separately refined using the delay and Doppler profiles. The delay profile is obtained from the k -th column of the received delay-Doppler matrix [16], [17]:

$$\mathbf{u} = [\mathbf{Y}_{dd}]_{:, n_p+\hat{k}} = \mathbf{Y}_{dd} \mathbf{e}_{n_p+\hat{k}} \in \mathbb{C}^M. \quad (30)$$

Similarly, the Doppler profile is obtained from the l -th row of the received delay-Doppler matrix:

$$\mathbf{v} = [\mathbf{Y}_{dd}]_{m_p, :} = \mathbf{Y}_{dd}^\top \mathbf{e}_{m_p+\hat{l}} \in \mathbb{C}^N. \quad (31)$$

The delay-Doppler matrix can be decomposed as

$$\mathbf{Y}_{dd} = \mathbf{Y}_{dd}^{\text{pilot}} + \mathbf{Y}_{dd}^{\text{data}} + \mathbf{N}_{dd}, \quad (32)$$

where

$$\mathbf{Y}_{dd}^{\text{pilot}} = \alpha \sigma_p \tilde{\mathbf{C}}(\nu) \mathbf{F}_M^H \left[\mathbf{F}_M \mathbf{P} \mathbf{F}_N^H \odot \mathbf{b}(\tau) \mathbf{c}^\top(\nu) \right] \mathbf{F}_N, \quad (33)$$

$$\mathbf{Y}_{dd}^{\text{data}} = \alpha \sigma_d \tilde{\mathbf{C}}(\nu) \mathbf{F}_M^H \left[\mathbf{D} \odot \mathbf{b}(\tau) \mathbf{c}^\top(\nu) \right] \mathbf{F}_N. \quad (34)$$

The delay profile can then be expressed as

$$\mathbf{u} = (\mathbf{Y}_{dd}^{\text{pilot}} + \mathbf{Y}_{dd}^{\text{data}}) \mathbf{e}_{n_p+\hat{k}} + \mathbf{n}_u, \quad (35)$$

where $\mathbf{n}_u \sim \mathcal{CN}(\mathbf{0}, \sigma^2 \mathbf{I}_M)$. Specifically,

$$\begin{aligned} & \mathbf{Y}_{dd}^{\text{pilot}} \mathbf{e}_{n_p+\hat{k}} \\ &= \alpha \sigma_p \tilde{\mathbf{C}}(\nu) \mathbf{F}_M^H \left[\mathbf{F}_M \mathbf{P} \mathbf{F}_N^H \odot \mathbf{b}(\tau) \mathbf{c}^\top(\nu) \right] \underbrace{\mathbf{F}_N \mathbf{e}_{n_p+\hat{k}}}_{\mathbf{f}_{n_p+\hat{k}}} \\ &= \alpha \sigma_p \tilde{\mathbf{C}}(\nu) \mathbf{F}_M^H \left[\underbrace{\mathbf{F}_M \mathbf{e}_{m_p}}_{\mathbf{f}_{m_p}} \underbrace{\mathbf{e}_{n_p}^\top \mathbf{F}_N^H}_{(\mathbf{f}_{n_p}^*)^\top} \odot \mathbf{b}(\tau) \mathbf{c}^\top(\nu) \right] \mathbf{f}_{n_p+\hat{k}} \\ &= \alpha \sigma_p \tilde{\mathbf{C}}(\nu) \mathbf{F}_M^H \left[\mathbf{f}_{m_p} \odot \mathbf{b}(\tau) \right] \underbrace{\left[\mathbf{f}_{n_p}^* \odot \mathbf{c}(\nu) \right]^\top}_{R_u} \mathbf{f}_{n_p+\hat{k}} \\ &= \alpha \sigma_p R_u \tilde{\mathbf{C}}(\nu) \underbrace{\mathbf{F}_M^H (\mathbf{f}_{m_p} \odot \mathbf{b}(\tau))}_{\text{delay term}}. \end{aligned} \quad (36)$$

The correlation term R_u represents a Doppler filtering process that extracts delay signals in the \hat{k} -th Doppler bin. The delay can then be estimated by correlating the delay profile with the delay term [16], [17]:

$$\hat{\tau} = \arg \max_{\tau} \left| \mathbf{u}^\top \mathbf{F}_M^H (\mathbf{f}_{m_p} \odot \mathbf{b}(\tau)) \right|. \quad (37)$$

This procedure allows refining the delay estimate in a neighborhood around $\hat{l}/(M\Delta f)$.

Similarly, the Doppler profile is obtained as

$$\mathbf{v} = (\mathbf{Y}_{dd}^{\text{pilot}} + \mathbf{Y}_{dd}^{\text{data}})^\top \mathbf{e}_{m_p+\hat{l}} + \mathbf{n}_v, \quad (38)$$

where $\mathbf{n}_v \sim \mathcal{CN}(\mathbf{0}, \sigma^2 \mathbf{I}_N)$. Specifically,

$$\begin{aligned}
& \mathbf{Y}_{dd}^{\text{pilot}\top} \mathbf{e}_{m_p+\hat{l}} \\
&= \alpha \sigma_p \mathbf{F}_N \left[\mathbf{F}_M \mathbf{P} \mathbf{F}_N^H \odot \mathbf{b}(\tau) \mathbf{c}^\top(\nu) \right]^\top \underbrace{\mathbf{F}_M^H \tilde{\mathbf{C}}(\nu) \mathbf{e}_{m_p+\hat{l}}}_{\approx \mathbf{F}_M^H \mathbf{e}_{m_p+\hat{l}} = \mathbf{f}_{m_p+\hat{l}}} \\
&\approx \alpha \sigma_p \mathbf{F}_N \left[\mathbf{F}_N^H \mathbf{P}^\top \mathbf{F}_M \odot \mathbf{c}(\nu) \mathbf{b}^\top(\tau) \right] \mathbf{f}_{m_p+\hat{l}} \\
&= \alpha \sigma_p \mathbf{F}_N \left[\mathbf{F}_N^H \mathbf{e}_{n_p} \mathbf{e}_{m_p}^\top \mathbf{F}_M \odot \mathbf{c}(\nu) \mathbf{b}^\top(\tau) \right] \mathbf{f}_{m_p+\hat{l}} \\
&= \alpha \sigma_p \mathbf{F}_N \left[\mathbf{f}_{n_p}^* \odot \mathbf{c}(\nu) \right] \underbrace{\left[\mathbf{f}_{m_p} \odot \mathbf{b}(\tau) \right]^\top}_{R_v} \mathbf{f}_{m_p+\hat{l}} \\
&= \alpha \sigma_p R_v \underbrace{\mathbf{F}_N \left(\mathbf{f}_{n_p}^* \odot \mathbf{c}(\nu) \right)}_{\text{Doppler term}}. \tag{39}
\end{aligned}$$

The correlation term R_v represents a delay filtering process that extracts Doppler signals in the \hat{l} -th delay bin. Similarly to the delay case, the Doppler can be refined by correlating the Doppler profile with the Doppler term [16], [17]:

$$\hat{\nu} = \arg \max_{\nu} \left| \mathbf{v}^H \mathbf{F}_N \left(\mathbf{f}_{n_p}^* \odot \mathbf{c}(\nu) \right) \right|. \tag{40}$$

This procedure refines the Doppler estimate in a neighborhood around $\hat{k}/(NT')$. Once the delay and Doppler are estimated, the optimal channel gain is obtained via LS as

$$\hat{\alpha} = \arg \min_{\alpha} \left\| \mathbf{R} - \alpha \mathbf{A}(\hat{\tau}, \hat{\nu}) \right\|_F^2, \tag{41}$$

where

$$\mathbf{A}(\tau, \nu) = \sigma_p \tilde{\mathbf{C}}(\nu) \mathbf{F}_M^H \left(\mathbf{F}_M \mathbf{P} \mathbf{F}_N^H \odot \mathbf{b}(\tau) \mathbf{c}^\top(\nu) \right). \tag{42}$$

Solving (41), the optimal gain is

$$\hat{\alpha} = \frac{\text{Tr}(\mathbf{A}^H(\hat{\tau}, \hat{\nu}) \mathbf{R})}{\left\| \mathbf{A}(\hat{\tau}, \hat{\nu}) \right\|_F^2}. \tag{43}$$

2) *Multipath Scenario*: In the case of multiple paths, the channel parameters of each path are estimated sequentially [16]–[19] using the residual delay-Doppler matrix $\mathcal{E}_{dd}^{(p)}$. In the first iteration, $\mathcal{E}_{dd}^{(0)} = \mathbf{Y}_{dd}$. During the p -th iteration, the delay and Doppler of the p -th path are initialized by searching for the maximum pilot energy in the residual delay-Doppler matrix $\mathcal{E}_{dd}^{(p-1)}$ as in (29). Subsequently, the delay and Doppler are separately refined using (37) and (40) within a neighborhood of $\hat{l}_p/M\Delta f$ and \hat{k}_p/NT' , respectively. The channel gain is then estimated from (43) as

$$\hat{\alpha}_p = \frac{\text{Tr}(\mathbf{A}^H(\hat{\tau}_p, \hat{\nu}_p) \mathcal{E}_{dd}^{(p-1)} \mathbf{F}_N^H)}{\left\| \mathbf{A}(\hat{\tau}_p, \hat{\nu}_p) \right\|_F^2}. \tag{44}$$

Once the parameters of a path are obtained, the next path is estimated on the updated residual matrix

$$\mathcal{E}_{dd}^{(p)} = \mathcal{E}_{dd}^{(p-1)} - \hat{\alpha}_p \mathbf{A}(\hat{\tau}_p, \hat{\nu}_p) \mathbf{F}_N. \tag{45}$$

This subtraction removes the contribution of the current path and mitigates interpath interference (IPI) arising from fractional effects [16]–[19]. The iterative procedure continues until

Algorithm 1: Proposed Fractional CE Algorithm

Input: \mathbf{Y}_{dd} , \mathbf{P} , P_{\max} , ϵ
 $\mathcal{E}_{dd}^{(0)} = \mathbf{Y}_{dd}$;
for $p = 1$ **to** P_{\max} **do**
 $\hat{l}_p, \hat{k}_p = \arg \max_{l,k} \left| \left[\mathcal{E}_{dd}^{(p-1)} \right]_{m_p+l, n_p+k} \right|^2$;
 $\mathbf{u} = \left[\mathcal{E}_{dd}^{(p-1)} \right]_{:, n_p+\hat{k}_p};$
 $\hat{\tau}_p = \arg \max_{\tau} \left| \mathbf{u}^H \mathbf{F}_M^H (\mathbf{f}_{m_p} \odot \mathbf{b}(\tau)) \right|$;
 $\mathbf{v} = \left[\mathcal{E}_{dd}^{(p-1)} \right]_{m_p+\hat{l}_p,:};$
 $\hat{\nu}_p = \arg \max_{\nu} \left| \mathbf{v}^H \mathbf{F}_N (\mathbf{f}_{n_p}^* \odot \mathbf{c}(\nu)) \right|$;
 $\hat{\alpha}_p = \frac{\text{Tr}(\mathbf{A}^H(\hat{\tau}_p, \hat{\nu}_p) \mathcal{E}_{dd}^{(p-1)} \mathbf{F}_N^H)}{\left\| \mathbf{A}(\hat{\tau}_p, \hat{\nu}_p) \right\|_F^2}$;
 $\mathcal{E}_{dd}^{(p)} = \mathcal{E}_{dd}^{(p-1)} - \hat{\alpha}_p \mathbf{A}(\hat{\tau}_p, \hat{\nu}_p) \mathbf{F}_N$;
if $\left\| \mathcal{E}_{dd}^{(p)} - \mathcal{E}_{dd}^{(p-1)} \right\|_F < \epsilon$ **then**
 $\hat{P} = p$;
break;
Output: $\{\hat{\alpha}_p, \hat{\tau}_p, \hat{\nu}_p\}_{p=1}^{\hat{P}}$;

either a maximum number of paths P_{\max} is estimated or the stopping criterion

$$\left\| \mathcal{E}_{dd}^{(p)} - \mathcal{E}_{dd}^{(p-1)} \right\|_F < \epsilon, \tag{46}$$

for a small arbitrary ϵ , is satisfied. The total number of detected paths is then $\hat{P} = \min(p, P_{\max})$.

The proposed multipath estimation approach is summarized in Algorithm 1.

IV. SYMBOL DETECTION

Assuming knowledge of the CSI, this section reviews conventional detection schemes and introduces the proposed iterative method for symbol detection. Specifically, the goal of symbol detection is to estimate the time-frequency symbol matrix \mathbf{X} . In the case of SP, after estimating the time-frequency symbol matrix according to the model in (21), an estimate of the data symbols is obtained by removing the pilot contribution as

$$\hat{\mathbf{D}} = \frac{\hat{\mathbf{X}} - \sigma_p \mathbf{F}_M \mathbf{P} \mathbf{F}_N^H}{\sigma_d}. \tag{47}$$

A. Baseline Methods

1) *Single-Tap MMSE (ICI-free)*: Under the assumption of negligible ICI, the model in (12) applies. The receiver can perform single-tap MMSE equalization to estimate \mathbf{X} as

$$\hat{\mathbf{X}} = \frac{\mathbf{H}_{tf}^* \odot \mathbf{Y}}{|\mathbf{H}_{tf}|^2 + \text{SNR}^{-1}}. \tag{48}$$

The overall complexity of this approach for the entire OFDM frame is $\mathcal{O}(MN)$.

Algorithm 2: Proposed IMFC Equalizer based on Landweber Method

Input: $\mathbf{R}, \left\{ \mathbf{H}_{tf}^{(p)}, \mathbf{H}_{\text{ICI}}^{(p)}, \alpha_p \right\}_{p=1}^P, \eta$

$\hat{\mathbf{X}}^{(0)} = \mathbf{0}$;

$\mathbf{E}^{(0)} = \mathbf{R}$;

for $t = 1$ **to** T **do**

$\Delta\hat{\mathbf{X}}^{(t)} = \mathbf{0}$;

for $p = 1$ **to** P **do**

$$\begin{cases} \hat{\mathbf{X}}_p^{(t)} \leftarrow \mathbf{E}^{(t-1)} \odot \left(\mathbf{H}_{\text{ICI}}^{(p)} \right)^*; \\ \hat{\mathbf{X}}_p^{(t)} \leftarrow \mathbf{F}_M \hat{\mathbf{X}}_p^{(t)}; \\ \hat{\mathbf{X}}_p^{(t)} \leftarrow \hat{\mathbf{X}}_p^{(t)} \odot \left(\mathbf{H}_{tf}^{(p)} \right)^*; \\ \Delta\hat{\mathbf{X}}^{(t)} \leftarrow \Delta\hat{\mathbf{X}}^{(t)} + \alpha_p^* \hat{\mathbf{X}}_p^{(t)}; \end{cases}$$

$\hat{\mathbf{X}}^{(t)} = \hat{\mathbf{X}}^{(t-1)} + \eta \Delta\hat{\mathbf{X}}^{(t)}$;

$\mathbf{E}^{(t)} = \mathbf{R}$;

for $p = 1$ **to** P **do**

$$\begin{cases} \mathbf{E}_p^{(t)} \leftarrow \hat{\mathbf{X}}^{(t)} \odot \mathbf{H}_{tf}^{(p)} \\ \mathbf{E}_p^{(t)} \leftarrow \mathbf{F}_M^H \mathbf{E}_p^{(t)}; \\ \mathbf{E}_p^{(t)} \leftarrow \mathbf{E}_p^{(t)} \odot \mathbf{H}_{\text{ICI}}^{(p)}; \\ \mathbf{E}^{(t)} \leftarrow \mathbf{E}^{(t)} - \alpha_p \cdot \mathbf{E}_p^{(t)}; \end{cases}$$

Output: $\hat{\mathbf{X}}^{(T)}$;

2) *Full MMSE (ICI-aware):* For non-negligible ICI, the receiver must perform full MMSE equalization [10], [11] to compensate for the loss of orthogonality between subcarriers

$$\hat{\mathbf{x}}_n = \left(\mathbf{H}_{tf,n}^H \mathbf{H}_{tf,n} + \text{SNR}^{-1} \mathbf{I}_M \right)^{-1} \mathbf{H}_{tf,n}^H \mathbf{y}_n, \quad (49)$$

where $\mathbf{y}_n = \mathbf{F}_M \mathbf{r}_n$ and $\mathbf{H}_{tf,n} = \mathbf{F}_M \mathbf{H}_n \mathbf{F}_M^H$. The estimates are then concatenated as $\hat{\mathbf{X}} = [\hat{\mathbf{x}}_0 \ \hat{\mathbf{x}}_1 \ \dots \ \hat{\mathbf{x}}_{N-1}]$.

The overall complexity of full MMSE detection for the entire OFDM frame is $\mathcal{O}(NM^3)$ due to the matrix inversion.

B. Proposed Reduced-Complexity Least Squares Detection via Landweber Method

This section introduces the proposed low-complexity equalizer based on the Landweber method, referred to as IMFC. The LS detection problem is formulated as

$$\hat{\mathbf{X}} = \arg \min_{\mathbf{X}} \left\| \mathbf{R} - \mathcal{H}(\mathbf{X}) \right\|_F^2. \quad (50)$$

Given the problem in (50), the Landweber iterative update is

$$\hat{\mathbf{X}}^{(t)} = \hat{\mathbf{X}}^{(t-1)} + \eta \mathcal{H}^H \left(\mathbf{R} - \mathcal{H}(\hat{\mathbf{X}}^{(t-1)}) \right), \quad (51)$$

where η is the step-size parameter and the initial estimate is $\hat{\mathbf{X}}^{(0)} = \mathbf{0}$. It can be noted that the learning rate η must be properly selected to guarantee convergence of the Landweber iteration [33]. In practice, η can be chosen empirically or adapted through a decay model, in accordance with standard results on iterative reconstruction methods. Exploiting the structure of the channel operator $\mathcal{H}(\cdot)$, the method can be decomposed into low-complexity path-wise operations. During the t -th iteration, the algorithm performs the following steps:

TABLE I: Simulation parameters.

General	
Carrier frequency, f_c	5.9 GHz
Number of subcarriers, M	128
Number of OFDM symbols, N	32
Subcarrier spacing, Δf	30 kHz
CP duration, T_{CP}	5 μ s
Modulation	QAM, $Q = 4, 16$
Wireless channel	
Number of multipaths, P	4
Propagation delays, τ_p	$[0, 0.9, 2.7, 4]$ μ s
Power delay profile	Uniform
Doppler shifts, ν_p	$\nu_p = f_c \frac{v_{\text{max}}}{c} \cos(\theta)$ $\theta \sim \mathcal{U}[0, 2\pi]$

1) *Single-Tap ICI Compensation in Delay-Time Domain:*

$$\hat{\mathbf{X}}_p^{(t)} \leftarrow \mathbf{E}^{(t-1)} \odot \left(\mathbf{H}_{\text{ICI}}^{(p)} \right)^*. \quad (52)$$

2) *Conversion to Frequency-Time Domain:*

$$\hat{\mathbf{X}}_p^{(t)} \leftarrow \mathbf{F}_M \hat{\mathbf{X}}_p^{(t)}. \quad (53)$$

3) *Single-Tap Frequency-Time Channel Equalization:*

$$\hat{\mathbf{X}}_p^{(t)} \leftarrow \hat{\mathbf{X}}_p^{(t)} \odot \left(\mathbf{H}_{tf}^{(p)} \right)^*. \quad (54)$$

4) *Combining:* The P path-wise estimates $\hat{\mathbf{X}}_p^{(t)}$ are combined using maximum ratio combining (MRC) to maximize the SNR:

$$\Delta\hat{\mathbf{X}}^{(t)} = \sum_{p=1}^P \alpha_p^* \hat{\mathbf{X}}_p^{(t)}. \quad (55)$$

The Landweber update is then applied as

$$\hat{\mathbf{X}}^{(t)} = \hat{\mathbf{X}}^{(t-1)} + \eta \Delta\hat{\mathbf{X}}^{(t)}, \quad (56)$$

and the residual observation matrix is updated as

$$\mathbf{E}^{(t)} = \mathbf{R} - \mathcal{H}(\hat{\mathbf{X}}^{(t)}), \quad (57)$$

and it can be noted that $\mathbf{E}^{(0)} = \mathbf{R}$ since the symbol matrix is initialized as zero.

The pseudocode of the proposed IMFC method is provided in Algorithm 2. The overall complexity of this iterative procedure, assuming $\log_2 M < N$, is dominated by the single-tap operations and scales as $\mathcal{O}(TPMN)$, where T is the number of iterations.

V. SIMULATION RESULTS

This section presents the simulation results used to validate the proposed receiver architecture. The main simulation parameters are listed in Table I. Two different channel models are considered:

- **Fractional channel:** This channel model resembles a realistic environment with fractional delays and Doppler shifts. Channel parameters are as listed in Table I.
- **Integer channel:** This channel assumes integer delays and Doppler shifts and is used to compare the proposed scheme against the baseline method in [3], which relies on this assumption. The channel parameters are obtained from Table I as

$$\tau_p^{\text{int}} = \frac{\text{round}(\tau_p M \Delta f)}{M \Delta f}, \quad \nu_p^{\text{int}} = \frac{\text{round}(\nu_p N T')}{N T'}. \quad (58)$$

TABLE II: Complexity comparison of the different methods.

Method	CE	Equalization
TM + Full MMSE	$\mathcal{O}(MN)$	$\mathcal{O}(NM^3)$
Prop. CE + Full MMSE	$\mathcal{O}(P_{\max} MN)$	$\mathcal{O}(NM^3)$
Perf. CSI + Full MMSE	-	$\mathcal{O}(NM^3)$
TM + Single-Tap	$\mathcal{O}(MN)$	$\mathcal{O}(MN)$
EP + Single-Tap	$\mathcal{O}(MN)$	$\mathcal{O}(MN)$
Prop. CE + Prop. IMFC	$\mathcal{O}(P_{\max} MN)$	$\mathcal{O}(TPMN)$

The following receiver architectures are considered for numerical evaluation:

- **TM + Full MMSE:** Channel estimation via the TM method [3] using the delay-Doppler SP scheme and equalization via the ICI-aware full MMSE equalizer.
- **Prop. CE + Full MMSE:** Channel estimation via the proposed fractional estimation method (Algorithm 1) with the delay-Doppler SP scheme, equalization via the ICI-aware full MMSE equalizer.
- **Perf. CSI + Full MMSE:** Delay-Doppler SP scheme is adopted at the transmitter, perfect CSI is assumed at the receiver, and equalization is performed using the ICI-aware full MMSE equalizer. This serves as an upper bound on communication performance.
- **TM + Single-Tap:** Channel estimation via the TM method with the delay-Doppler SP scheme and ICI-free single-tap MMSE equalization. This corresponds to the baseline receiver in [3].
- **EP + Single-Tap:** Channel estimation via conventional EP in OFDM systems and equalization via the ICI-free single-tap MMSE equalizer.
- **Prop. CE + Prop. IMFC:** Channel estimation via the proposed fractional estimation method (Algorithm 1) with the delay-Doppler SP scheme and equalization via the proposed ICI-aware IMFC equalizer.

A complexity comparison of all schemes is provided in Table II. It can be observed that the TM + Single-Tap and conventional EP + Single-Tap schemes have the lowest complexity, at the cost of neglecting ICI and fractional effects. In contrast, the Prop. CE + Prop. IMFC scheme has higher complexity but remains linear in the number of REs, unlike full MMSE-based receivers, whose equalization complexity scales cubically with the number of OFDM subcarriers.

A. Peak-to-Average Power Ratio

The peak-to-average power ratio (PAPR) is a critical metric in modern wireless systems, particularly for multi-carrier schemes. High PAPR increases the linearity requirements of the power amplifiers (PA), forcing it to operate with a large power back-off. This reduces efficiency, increases energy consumption, and may introduce non-linear distortion that degrades signal reliability and spectral purity. Therefore, evaluating the PAPR of different transmission schemes is essential for assessing their practical feasibility in real-world deployments. The PAPR is defined as

$$\text{PAPR} = \frac{\max_{m,n} |[\mathbf{S}]_{m,n}|^2}{P_T}. \quad (59)$$

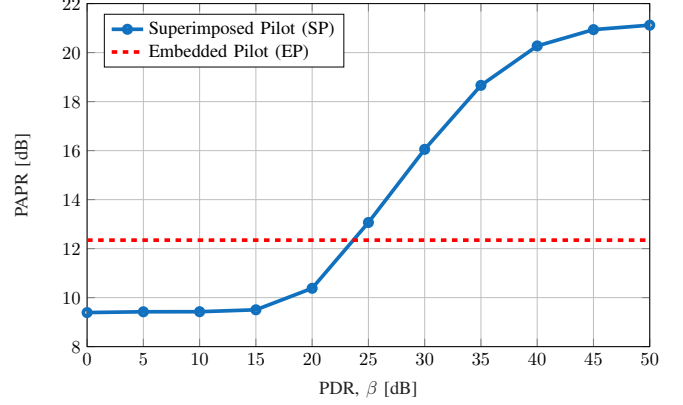


Fig. 2: The PAPR of the delay-Doppler SP-based scheme is shown for different values of PDR and compared against the PAPR of the EP-based scheme

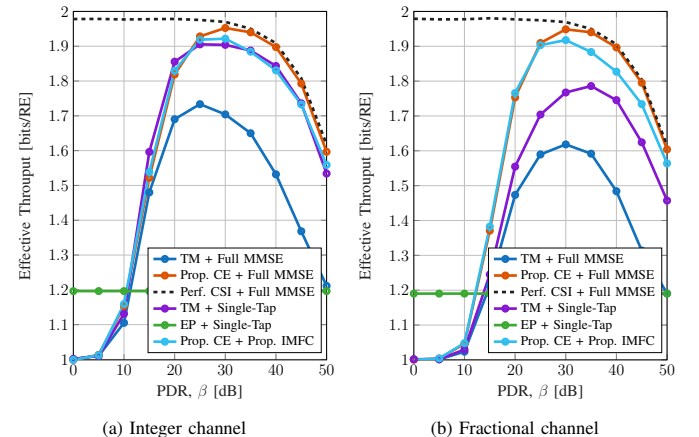


Fig. 3: Effective throughput against PDR for a fixed SNR of 15 dB. The modulation order is $Q = 4$ and the maximum speed is 1000 km/h.

Figure 2 reports the PAPR of the delay-Doppler SP scheme for different values of the PDR. The PAPR of the conventional EP scheme is also shown for comparison. It can be observed that for PDR values below 23 dB, the SP scheme exhibits a lower PAPR than the EP scheme, with a minimum PAPR slightly below 10 dB. Conversely, for higher PDR values, the PAPR increases and can reach up to 21 dB.

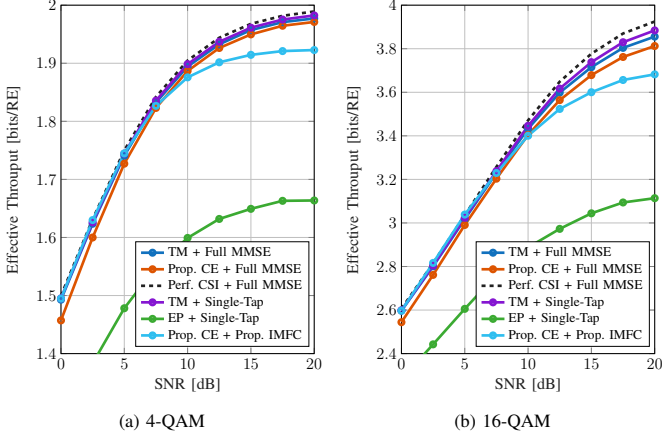
B. Communication Performance Metrics

To fairly compare different pilot schemes (SP and EP) that use time-frequency and power resources differently, the *effective throughput* η_{eff} is adopted as the main communication performance metric [3], [21]. The receiver is assumed to select the CE and symbol detection method that maximizes η_{eff} . For the considered uncoded system, the effective throughput is defined as [3]

$$\eta_{\text{eff}} = (1 - \text{BER})\mathcal{D} \log_2 Q, \quad (60)$$

where BER is the bit error rate, Q is the modulation order, and \mathcal{D} is the data density. The data density is given by

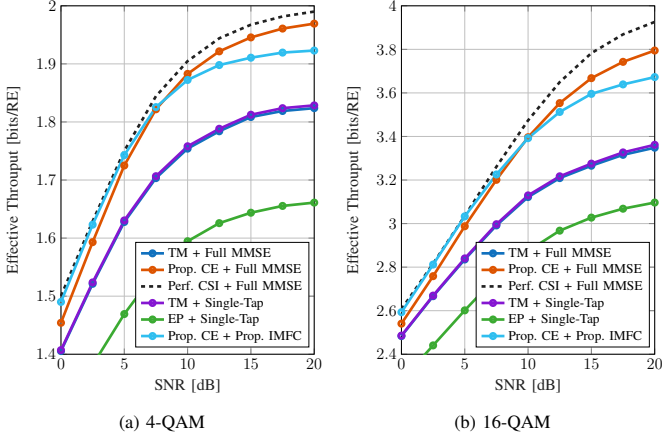
$$\mathcal{D} = \begin{cases} 1, & \text{SP,} \\ 1 - \mathcal{D}_p = 1 - \frac{1}{K_t K_f}, & \text{EP.} \end{cases} \quad (61)$$



(a) 4-QAM

(b) 16-QAM

Fig. 4: Effective throughput against SNR for a fixed PDR of 30 dB. The channel has integer delays and Doppler shifts and the maximum speed is 100 km/h.



(a) 4-QAM

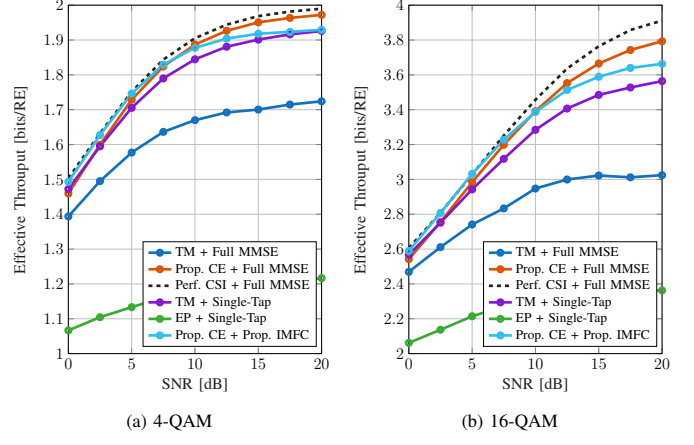
(b) 16-QAM

Fig. 5: Effective throughput against SNR for a fixed PDR of 30 dB. The channel has fractional delays and Doppler shifts and the maximum speed is 100 km/h.

In particular, for conventional EP schemes, $\mathcal{D}_p \neq 0$ and thus $\mathcal{D} < 1$ since some REs are reserved for pilots. For SP schemes $\mathcal{D} = 1$, as all time-frequency resources carry data [3].

C. Optimum PDR Selection

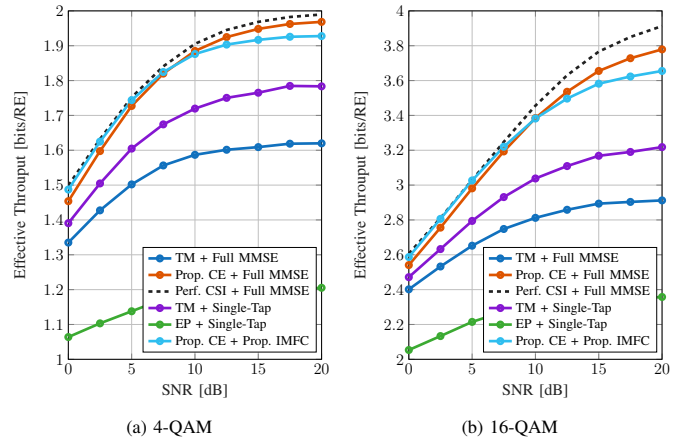
Given the SP scheme discussed in Section III-B, it can be noted that the PDR governs the trade-off between CE accuracy and data detection quality. For a fixed transmit power P_T , increasing the PDR boosts the pilot amplitude, improving channel estimation [3], but reduces the power allocated to data symbols, thereby degrading the detection SNR. Conversely, lowering the PDR enhances the detection SNR but reduces pilot power, leading to poorer CE accuracy. This intrinsic trade-off results in an optimal PDR that maximizes effective throughput. Figure 3 illustrates that all delay-Doppler SP-based methods achieve their highest η_{eff} at specific PDR values. In particular, the optimum PDR that maximizes effective throughput is approximately 30 dB. Deviating from this value, either by increasing or decreasing the PDR, causes η_{eff} to drop, eventually falling below that of the conventional EP + Single-Tap scheme.



(a) 4-QAM

(b) 16-QAM

Fig. 6: Effective throughput against SNR for a fixed PDR of 30 dB. The channel has integer delays and Doppler shifts and the maximum speed is 1000 km/h.



(a) 4-QAM

(b) 16-QAM

Fig. 7: Effective throughput against SNR for a fixed PDR of 30 dB. The channel has fractional delays and Doppler shifts and the maximum speed is 1000 km/h.

D. Effective Throughput vs SNR

The communication performance is evaluated for both integer and fractional channel models. Figures 4 and 5 show the effective throughput for 4-QAM and 16-QAM under integer and fractional channel parameters, respectively. The maximum speed is 100 km/h, so that ICI is negligible. It can be observed that delay-Doppler SP schemes consistently outperform the conventional EP-based scheme. In particular, Figure 4 shows that the TM + Single-Tap method [3] achieves performance close to the Perf. CSI + Full MMSE bound when channel parameters are integers. In contrast, for the more realistic fractional channel in Figure 5, the TM + Single-Tap performance degrades significantly due to the violation of the integer assumption. The proposed Prop. CE + Prop. IMFC scheme, instead, achieves performance close to the Perf. CSI + Full MMSE bound in both integer and fractional scenarios, outperforming the TM + Single-Tap baseline when fractional channel parameters are present. Furthermore, in both Figures 4 and 5, the Prop. CE + Prop. IMFC has comparable performance to that of the Prop. CE + Full MMSE, except for a small drop at high SNR values, indicating that the proposed

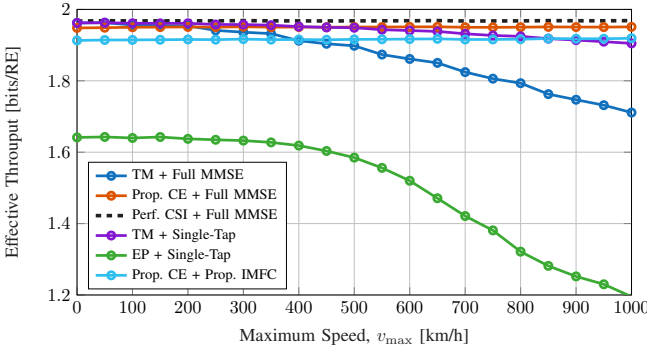


Fig. 8: Effective throughput against maximum channel speed for a fixed PDR of 30 dB and SNR of 15 dB. The channel has integer delays and Doppler shifts and the transmitter adopts the 4-QAM.

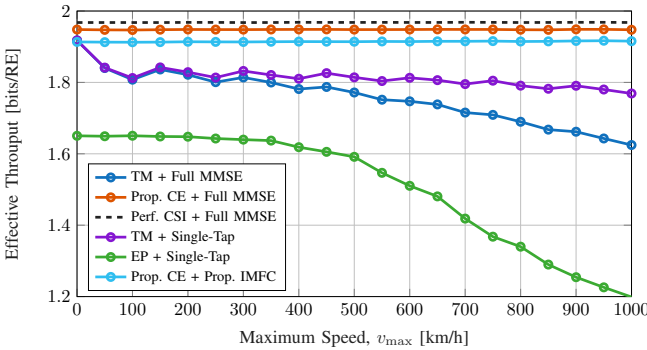


Fig. 9: Effective throughput against maximum channel speed for a fixed PDR of 30 dB and SNR of 15 dB. The channel has fractional delays and Doppler shifts and the transmitter adopts the 4-QAM.

iterative detection scheme achieves high effective throughput at much lower computational complexity (linear in M versus cubic for full MMSE).

Figures 6 and 7 depict the performance at a higher mobility scenario with maximum speed of 1000 km/h, representative of extreme 6G conditions. In this case, the Prop. CE + Prop. IMFC outperforms the TM + Single-Tap in both integer and fractional channels, as ICI becomes non-negligible. The TM + Single-Tap method fails to compensate for ICI, while the proposed approach accounts for both ICI and fractional delays/Doppler shifts, maintaining robust performance. The performance gap is especially pronounced for fractional channels, highlighting the advantage of the proposed method under realistic conditions. Overall, Prop. CE + Prop. IMFC remains closer to the Perf. CSI + Full MMSE bound across all considered scenarios.

Interestingly, Figures 6 and 7 also show that TM + Single-Tap outperforms TM + Full MMSE despite ICI being non-negligible. This is because the TM-based CE method does not model ICI, while the full MMSE equalizer attempts to compensate for it. The mismatch leads to suboptimal performance for TM + Full MMSE, whereas the ICI-free TM + Single-Tap yields better throughput under these conditions.

E. Effective Throughput vs Speed

To evaluate robustness under varying mobility conditions expected in 6G, Figures 8 and 9 illustrate the effective through-

put as a function of maximum channel speed for integer and fractional channels, respectively. In Figure 8, the TM + Single-Tap method achieves near-optimal performance across all speeds, exhibiting only a minor throughput degradation even at very high mobility. The Prop. CE + Prop. IMFC method shows slightly lower throughput compared to TM + Single-Tap and Prop. CE + Full MMSE in this idealized integer channel scenario, due to the additional processing required to account for fractional effects that are absent here. Figure 9 presents a more realistic scenario with fractional channel parameters. Here, the TM + Single-Tap method starts to fail even at moderate speeds. While it matches the throughput of Prop. CE + Prop. IMFC in static channels ($v_{\max} = 0$), its performance rapidly degrades as the maximum speed increases due to high IPI resulting from fractional delays and Doppler shifts. Conversely, the Prop. CE + Prop. IMFC maintains a nearly constant effective throughput across the entire speed range, demonstrating robust performance under high-mobility conditions. This highlights the suitability of the proposed method for practical high-speed OFDM communications, where both fractional channel effects and ICI are present.

VI. CONCLUSIONS AND FUTURE WORKS

In this work, a novel receiver architecture for SISO OFDM high-mobility communications using delay-Doppler superimposed pilots has been proposed. The current literature on delay-Doppler SP largely relies on the assumptions of integer delays and Doppler shifts, as well as ICI-free operation. The proposed approach effectively addresses these limitations by: (i) enabling accurate estimation of fractional channel parameters, and (ii) incorporating ICI-aware receiver processing.

The receiver design maintains low complexity, leveraging disjoint delay-Doppler estimation and the Landweber-based IMFC equalizer, whose complexity scales linearly with the number of REs. Extensive simulation results demonstrate that the proposed approach achieves nearly constant communication performance across a wide range of mobility scenarios, up to the maximum 6G speed of 1000 km/h. These results highlight the potential of delay-Doppler SP schemes to enhance OFDM performance in future high-mobility 6G networks.

Future research directions include extending delay-Doppler SP algorithms to multi-antenna OFDM systems and exploring novel multiple superimposed pilot designs to reduce PAPR, which is a key limitation of the current single-pilot approach. Additionally, given that the delay-Doppler domain is naturally suited for sensing applications, the performance of OFDM with delay-Doppler SP in integrated sensing and communication (ISAC) systems will be investigated.

REFERENCES

- [1] L. Litwin and M. Pugel, "The principles of OFDM," *RF Signal Process*, vol. 2, pp. 30–48, 2001.
- [2] Y. Hong, T. Thaj, and E. Viterbo, *Delay-Doppler Communications: Principles and Applications*. Netherlands: Elsevier, 2022, publisher Copyright: © 2022 Elsevier Inc. All rights reserved.
- [3] Y. Bello, V. Corlay, and C. C. Duchesne, "A New Delay-Doppler-Based Pilot Scheme for OFDM Systems," in *2025 IEEE 101st Vehicular Technology Conference (VTC2025-Spring)*, 2025, pp. 1–7.

[4] M. Giordani, M. Polese, M. Mezzavilla, S. Rangan, and M. Zorzi, "Toward 6G Networks: Use Cases and Technologies," *IEEE Communications Magazine*, vol. 58, no. 3, pp. 55–61, 2020.

[5] H. Tataria, M. Shafi, A. F. Molisch, M. Dohler, H. Sjöland, and F. Tufvesson, "6G Wireless Systems: Vision, Requirements, Challenges, Insights, and Opportunities," *Proceedings of the IEEE*, vol. 109, no. 7, pp. 1166–1199, 2021.

[6] P. Robertson and S. Kaiser, "Analysis of the loss of orthogonality through Doppler spread in OFDM systems," in *Seamless Interconnection for Universal Services. Global Telecommunications Conference. GLOBECOM'99. (Cat. No.99CH37042)*, vol. 1B, 1999, pp. 701–706 vol. 1b.

[7] ———, "The effects of Doppler spreads in OFDM(A) mobile radio systems," in *Gateway to 21st Century Communications Village. VTC 1999-Fall. IEEE VTS 50th Vehicular Technology Conference (Cat. No.99CH36324)*, vol. 1, 1999, pp. 329–333 vol.1.

[8] Y. Mostofi and D. Cox, "ICI mitigation for pilot-aided OFDM mobile systems," *IEEE Transactions on Wireless Communications*, vol. 4, no. 2, pp. 765–774, 2005.

[9] T. Wang, J. Proakis, E. Masry, and J. Zeidler, "Performance degradation of OFDM systems due to Doppler spreading," *IEEE Transactions on Wireless Communications*, vol. 5, no. 6, pp. 1422–1432, 2006.

[10] Y.-S. Choi, P. Voltz, and F. Cassara, "On channel estimation and detection for multicarrier signals in fast and selective Rayleigh fading channels," *IEEE Transactions on Communications*, vol. 49, no. 8, pp. 1375–1387, 2001.

[11] Y. Ma, B. Ai, J. Yuan, S. Li, Q. Cheng, Z. Shi, W. Yuan, Z. Wei, A. Shafie, G. Ma, Y. Lu, M. Yang, and Z. Zhong, "Delay-Doppler Domain Signal Processing Aided OFDM (DD-a-OFDM) for 6G and Beyond," 2025. [Online]. Available: <https://arxiv.org/abs/2508.04253>

[12] Y. Zhou, H. Yin, J. Xiong, S. Song, J. Zhu, J. Du, H. Chen, and Y. Tang, "Overview and Performance Analysis of Various Waveforms in High Mobility Scenarios," in *2024 7th International Conference on Communication Engineering and Technology (ICCET)*, 2024, pp. 35–40.

[13] R. Hadani, S. Rakib, M. Tsatsanis, A. Monk, A. J. Goldsmith, A. F. Molisch, and R. Calderbank, "Orthogonal Time Frequency Space Modulation," in *2017 IEEE Wireless Communications and Networking Conference (WCNC)*, 2017, pp. 1–6.

[14] S. K. Mohammed, R. Hadani, A. Chockalingam, and R. Calderbank, "Otfs—a mathematical foundation for communication and radar sensing in the delay-doppler domain," *IEEE BITS the Information Theory Magazine*, vol. 2, no. 2, pp. 36–55, 2022.

[15] P. Raviteja, K. T. Phan, and Y. Hong, "Embedded Pilot-Aided Channel Estimation for OTFS in Delay-Doppler Channels," *IEEE Transactions on Vehicular Technology*, vol. 68, no. 5, pp. 4906–4917, 2019.

[16] I. A. Khan and S. K. Mohammed, "Low Complexity Channel Estimation for OTFS Modulation with Fractional Delay and Doppler," 2021.

[17] ———, "A Low-Complexity OTFS Channel Estimation Method for Fractional Delay-Doppler Scenarios," *IEEE Wireless Communications Letters*, vol. 12, no. 9, pp. 1484–1488, 2023.

[18] M. Marchese, H. Wymeersch, P. Spallaccini, and P. Savazzi, "Progressive Inter-Path Interference Cancellation Algorithm for Channel Estimation Using Orthogonal Time-Frequency Space," *Sensors*, vol. 24, no. 4414, 2024. [Online]. Available: <https://doi.org/10.3390/s24134414>

[19] M. Marchese, M. F. Keskin, P. Savazzi, and H. Wymeersch, "Disjoint Delay-Doppler Estimation in OTFS ISAC with Deep Learning-aided Path Detection," 2025. [Online]. Available: <https://arxiv.org/abs/2504.20659>

[20] H. B. Mishra, P. Singh, A. K. Prasad, and R. Budhiraja, "OTFS Channel Estimation and Data Detection Designs With Superimposed Pilots," *IEEE Transactions on Wireless Communications*, vol. 21, no. 4, pp. 2258–2274, 2022.

[21] Y. Kanazawa, H. Iimori, C. Pradhan, S. Malomsoky, and N. Ishikawa, "Superimposed Pilot-Based OTFS – Will it Work?" 2025. [Online]. Available: <https://arxiv.org/abs/2501.15935>

[22] S. Colieri, M. Ergen, A. Puri, and B. A, "A study of channel estimation in OFDM systems," in *Proceedings IEEE 56th Vehicular Technology Conference*, vol. 2, 2002, pp. 894–898 vol.2.

[23] S. Colieri, M. Ergen, A. Puri, and A. Bahai, "Channel estimation techniques based on pilot arrangement in OFDM systems," *IEEE Transactions on Broadcasting*, vol. 48, no. 3, pp. 223–229, 2002.

[24] T. Cui and C. Tellambura, "Pilot symbols for channel estimation in OFDM systems," in *GLOBECOM '05. IEEE Global Telecommunications Conference*, 2005, vol. 4, 2005, pp. 5 pp.–2233.

[25] A. R. Varma, C. R. N. Athaudage, L. L. H. Andrew, and J. H. Manton, "Optimal Superimposed Pilot Selection for OFDM Channel Estimation," in *2006 IEEE 7th Workshop on Signal Processing Advances in Wireless Communications*, 2006, pp. 1–5.

[26] S. Liu, J. Zhan, W. Xie, and F. Li, "Channel Estimation Using Frequency-domain Superimposed Pilot Time-Domain Correlation Method for OFDM Systems," in *2006 International Conference on Communication Technology*, 2006, pp. 1–4.

[27] S. Lu, G. Kang, Q. Zhu, and P. Zhang, "A Orthogonal Superimposed Pilot for Channel Estimation in MIMO-OFDM systems," in *2007 IEEE 65th Vehicular Technology Conference - VTC2007-Spring*, 2007, pp. 2409–2413.

[28] K. Josiam and D. Rajan, "Bandwidth Efficient Channel Estimation Using Super-Imposed Pilots in OFDM Systems," *IEEE Transactions on Wireless Communications*, vol. 6, no. 6, pp. 2234–2245, 2007.

[29] L. He, Y.-C. Wu, S. Ma, T.-S. Ng, and H. V. Poor, "Superimposed Training-Based Channel Estimation and Data Detection for OFDM Amplify-and-Forward Cooperative Systems Under High Mobility," *IEEE Transactions on Signal Processing*, vol. 60, no. 1, pp. 274–284, 2012.

[30] H. Zhang, H.-C. Wu, H. Jiang, and S. C.-H. Huang, "Robust pilot detection techniques for channel estimation and symbol detection in OFDM systems," in *2014 IEEE Global Communications Conference*, 2014, pp. 3025–3031.

[31] H. P. H. Shaw, J. Yuan, and M. Rowshan, "Delay-Doppler Channel Estimation by Leveraging the Ambiguity Function in OFDM Systems," in *2023 IEEE International Conference on Communications Workshops (ICC Workshops)*, 2023, pp. 307–313.

[32] H. P. H. Shaw, M. Rowshan, and J. Yuan, "Improving OFDM Using Delay-Doppler Channel Estimation," *IEEE Open Journal of the Communications Society*, vol. 6, pp. 7184–7199, 2025.

[33] C. Byrne, "A unified treatment of some iterative algorithms in signal processing and image reconstruction," *Inverse Problems*, vol. 20, no. 1, p. 103, nov 2003. [Online]. Available: <https://doi.org/10.1088/0266-5611/20/1/006>

[34] K.-C. Hung and D. W. Lin, "Jointly iterative channel estimation and data detection for cyclic-prefixed block transmission over time-varying channels," in *2007 6th International Conference on Information, Communications & Signal Processing*, 2007, pp. 1–5.

[35] M. F. Keskin, H. Wymeersch, and V. Koivunen, "MIMO-OFDM Joint Radar-Communications: Is ICI Friend or Foe?" *IEEE Journal of Selected Topics in Signal Processing*, vol. 15, no. 6, pp. 1393–1408, 2021.

[36] M. F. Keskin, C. Marcus, O. Eriksson, A. Alvarado, J. Widmer, and H. Wymeersch, "Integrated Sensing and Communications With MIMO-OTFS: ISI/ICI Exploitation and Delay-Doppler Multiplexing," *IEEE Transactions on Wireless Communications*, vol. 23, no. 8, pp. 10229–10246, 2024.